



Carreau fluid in a wall driven corner flow

S.T. Chaffin*, J.M. Rees

School of Mathematics and Statistics, University of Sheffield, Hicks Building, Hounsfield Road, Sheffield S3 7RH, UK

ARTICLE INFO

Keywords:

Carreau fluid
Wall driven corner flow
Matched asymptotic

ABSTRACT

Taylor's classical paint scraping problem provides a framework for analyzing wall-driven corner flow induced by the movement of an oblique plane with a fixed velocity U . A study of the dynamics of the inertialess limit of a Carreau fluid in such a system is presented. New perturbation results are obtained both close to, and far from, the corner. When the distance from the corner r is much larger than $U\Gamma$, where Γ is the relaxation time, a loss of uniformity arises in the solution near the region, where the shear rate becomes zero due to the presence of the two walls. We derive a new boundary layer equation and find two regions of widths r^{-n} and r^{-2} , where r is the distance from the corner and n is the power-law index, where a change in behavior occurs. The shear rate is found to be proportional to the perpendicular distance from the line of zero shear. The point of zero shear moves in the layer of size r^{-2} . We also find that Carreau effects in the far-field are important for corner angles less than 2.2 rad.

1. Introduction

Corner flows of both Newtonian and non-Newtonian fluids have been widely studied. Dean and Montagon [1] showed that for the flow of an inertialess Newtonian fluid, in plane polar coordinates (r, θ) , the stream function $\psi(r, \theta)$ permits similarity solutions of the form $r^\lambda f(\theta)$. They identified the existence of a critical corner angle for which λ becomes complex. Later Moffatt [2] correctly asserted that these complex values would give rise to an infinite series of eddies of decreasing size. An experimental study by Taneda [3] revealed the existence of a series of decreasing eddies, thus confirming Moffatt's theoretical predictions.

Following Moffatt's work, Proudman and Asadullah [4] considered the case of two inertialess immiscible Newtonian fluids of different viscosities with a planar contact line and found that the limit to a one phase system introduced an additional mode. Later, Henriksen and Hassager [5] studied power-law fluids in a corner region, though due to physical constraints imposed on the power-law model, the results were limited to the parameter regime $0 < n < 2$, where n is the power-law exponent. Likewise, Keiller and Hinch [6] examined a system suspension of rigid rods in a corner, but neglected the Brownian motion term of the constitutive equation in order to permit a similarity solution. They considered the aligned and unaligned orientations of the rods separately, but found that the solutions gave rise to unphysical eddies.

In this study, we consider a two-dimensional incompressible fluid that occupies the region between two semi-infinite planes (Fig. 1). One plane is moved with constant velocity U that drives the flow. The other plane is fixed at an angle α relative to the moving plane. In the vicinity

of the corner wall effects dominate, the flow and inertial terms become negligible so the creeping flow approximation can be used. This problem was first solved by Taylor [7]. Inertial effects were incorporated by Hancock et al. [8] by means of a perturbation expansion for the stream function. A study of the three-dimensional analogue of the paint scraping problem for a Newtonian fluid was first presented by Hills and Moffatt [9], motivated by the fact that this mechanism is used throughout the chemical process industry to induce mixing. The understanding of mixing in the chemical processing industry is of great importance as efficient mixing can improve consistency of products and reduce overall manufacturing costs [10,11]. As many industrial fluids exhibit non-Newtonian effects this motivates our further investigation into non-Newtonian fluids. The two-dimensional system has been analyzed for several types of non-Newtonian fluids. Riedler and Schneider [12] found an exact solution for a power-law fluid in the creeping flow regime, and further considered the effects of leakage at the apex of the corner. Analysis of this geometry is not limited to power-law fluids but can be applied to other constitutive relations [13]. The power-law model has the unphysical feature of having zero or infinite shear viscosity in regions where the shear rate tends to zero depending upon whether n is greater than or less than 1. Often an alternative model is needed to obtain correct physical behavior. The most commonly used alternative is the Carreau model, where the kinematic viscosity, ν , is given by

$$\nu = \nu_\infty + (\nu_0 - \nu_\infty)(1 + \Gamma^2 \dot{\gamma}^2)^{\frac{n-1}{2}}, \quad (1)$$

where $\dot{\gamma}$ is the generalized shear rate, Γ is the relaxation time and ν_∞

* Corresponding author.

E-mail address: s.chaffin@sheffield.ac.uk (S.T. Chaffin).

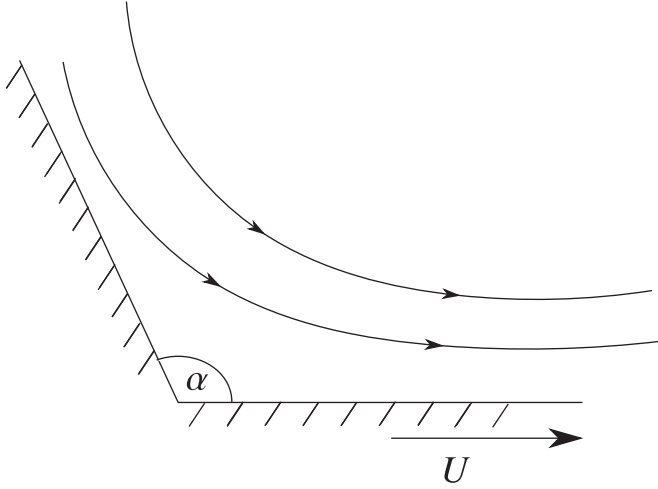


Fig. 1. Sketch of the driven corner flow system.

and ν_0 are the infinite shear and zero shear viscosities respectively. In the limit of low shear rates the viscosity approaches Newtonian behavior, thus overcoming the unphysical features of the power-law model. Throughout this article we will take $\nu_\infty = 0$, as this is a common assumption when fitting experimental data to the Carreau model [14].

A Carreau fluid exhibits increased complexity in a wall-driven corner flow in comparison to a power-law fluid. This arises as it transitions from exhibiting Newtonian behavior to power-law behavior in the geometry. The physics of this system does not permit a global self-similar solution, such as those that can be found for the cases of purely Newtonian or purely power-law fluids. As no global solution exists, our approach will be to consider the solution in two different domains: firstly, in the region far from the corner apex, where the shear rates are low and the solution is approximately Newtonian with a small power-law correction, and secondly, in the vicinity of the corner apex, where the behavior is predominantly power-law coupled with a small Newtonian effect. It is worth noting that a global solution can be found for situations where the shear-rate has no radial dependence. This scenario occurs for the shear-driven problem and is discussed later in Section 7.

The structure of this article is as follows. The governing equations, boundary conditions and perturbation approach are discussed in Section 2. Section 3 presents the analysis of the system far from the corner, and the analysis near to the corner is described in Section 4. The matching process associated with the arising boundary layer system is analyzed in Section 5. The importance of eigen-modes and far field conditions are discussed in Section 6. Conclusions and further discussion are given in Section 7.

2. Governing equations

The governing equations for the model are given by

$$\rho(\mathbf{u} \cdot \nabla) \mathbf{u} = -\nabla p + \nabla \cdot \boldsymbol{\tau}, \quad (2)$$

$$\nabla \cdot \mathbf{u} = 0, \quad (3)$$

where $\boldsymbol{\tau}$ is the viscous stress tensor given by $\boldsymbol{\tau} = \rho \nu \dot{\boldsymbol{\gamma}}$, where $\dot{\boldsymbol{\gamma}} = \nabla \mathbf{u} + \nabla \mathbf{u}^T$ is the rate of deformation tensor, ρ is the density and \mathbf{u} denotes the velocity field. The kinematic viscosity, ν , is given by (1) with the generalized shear rate $\dot{\boldsymbol{\gamma}}^2 = \frac{1}{2} \dot{\boldsymbol{\gamma}} : \dot{\boldsymbol{\gamma}}$. Under the scalings

$$\mathbf{u} = U \tilde{\mathbf{u}}, \quad r = U \Gamma \tilde{r}, \quad p = \frac{\rho \nu_0}{\Gamma} \tilde{p}, \quad \boldsymbol{\tau} = \frac{\rho \nu_0}{\Gamma} \tilde{\boldsymbol{\tau}}, \quad (4)$$

the system reduces to

$$Re(\tilde{\mathbf{u}} \cdot \tilde{\nabla}) \tilde{\mathbf{u}} = \tilde{\nabla} \cdot \tilde{\boldsymbol{\tau}} + \tilde{\nabla} \tilde{p}, \quad \tilde{\boldsymbol{\tau}} = \tilde{\nu}(\tilde{\boldsymbol{\gamma}}) \tilde{\boldsymbol{\gamma}} \quad (5)$$

Table 1

A collection of Carreau parameters for a range of fluids. Fluids A1 and A2 are polystyrene solutions with mass fractions 0.45 and 0.3, respectively [14]. Fluids A3 and A4 are wood flour polypropylene mixtures [15], with wood flour volume fractions of 0 and 0.28, respectively. The viscosity μ_0 is the dynamic viscosity which is related to the kinematic viscosity by $\nu_0 = \mu_0/\rho$.

Fluid	n	Γ (s)	μ_0 (Pa s)
A1	0.304	1.11	8.08
A2	0.305	0.03	135
A3	0.652	0.319	1.18×10^3
A4	0.0459	5.92	9.26×10^4

$$\tilde{\nabla} \cdot \tilde{\mathbf{u}} = 0, \quad (6)$$

where the scaled kinematic viscosity is given by $\tilde{\nu}(\tilde{\boldsymbol{\gamma}}) = (1 + \tilde{\boldsymbol{\gamma}}^2)^{\frac{n-1}{2}}$ and the Reynolds number is given by $Re = U^2 \Gamma / \nu_0$. Henceforth we assume that the Reynolds number is sufficiently small that the inertial terms are negligible. Using the parameters from Table 1 and assuming that all of the fluids have density of approximately 10^3 kg m^{-3} , we can obtain estimates for U for which the inertial terms can be neglected. The most restrictive case (fluid A1) requires that for inertia to be negligible $U \ll 0.1 \text{ m s}^{-1}$. The least restrictive case (fluid A4) gives the condition $U \ll 4 \text{ m s}^{-1}$. Henceforth, we drop tilde notation for convenience.

Mass conservation can be satisfied by the introduction of a stream-function Ω and the pressure can be eliminated by taking the curl of Eq. (5). Thus, the momentum equation can be expressed in terms of the stress tensor $\boldsymbol{\tau}$:

$$r^{-1} \left(-\frac{1}{r} \frac{\partial^2 \tau_{r\theta}}{\partial \theta^2} + \frac{\partial}{\partial r} \left\{ \frac{1}{r} \frac{\partial}{\partial r} (r^2 \tau_{r\theta}) \right\} + \frac{1}{r} \frac{\partial^2}{\partial r \partial \theta} \{ r(\tau_{\theta\theta} - \tau_{rr}) \} \right) = 0, \quad (7)$$

where the components of $\boldsymbol{\tau}$ are given in terms of the stream-function by

$$\tau_{rr} = -\tau_{\theta\theta} = 2\nu(\dot{\boldsymbol{\gamma}}) \frac{\partial}{\partial r} \left\{ \frac{1}{r} \frac{\partial \Omega}{\partial \theta} \right\}, \quad \tau_{r\theta} = \nu(\dot{\boldsymbol{\gamma}}) \left(\frac{1}{r^2} \frac{\partial^2 \Omega}{\partial \theta^2} - r \frac{\partial}{\partial r} \left\{ \frac{1}{r} \frac{\partial \Omega}{\partial r} \right\} \right), \quad (8)$$

$$\dot{\boldsymbol{\gamma}}^2 = 4 \left(\frac{\partial}{\partial r} \left\{ \frac{1}{r} \frac{\partial \Omega}{\partial \theta} \right\} \right)^2 + \left(\frac{1}{r^2} \frac{\partial^2 \Omega}{\partial \theta^2} - r \frac{\partial}{\partial r} \left\{ \frac{1}{r} \frac{\partial \Omega}{\partial r} \right\} \right)^2. \quad (9)$$

Eq. (7) is subject to no-slip and moving wall boundary conditions on the fixed and moving planes, respectively,

$$\begin{aligned} \Omega = 0, \quad \frac{1}{r} \frac{\partial \Omega}{\partial \theta} = 1, \quad \text{on } \theta = 0, \\ \Omega = 0, \quad \frac{\partial \Omega}{\partial \theta} = 0, \quad \text{on } \theta = \alpha. \end{aligned} \quad (10)$$

From the form of the boundary condition (10), if a global similarity solution were to exist one would expect $\Omega = r f(\theta)$. The problem with such an ansatz is that the radial viscosity behavior $\nu(\dot{\boldsymbol{\gamma}}) \sim (1 + r^{-1})^{\frac{n-1}{2}}$, and thus no similarity solution is permitted. We note that for large r the Newtonian effects dominate and that for small r shear-thinning effects dominate. At such scales the problem proves amenable to mathematical analysis. To distinguish between these regimes we will introduce a scaled radius $\mathcal{E}^{-1} R = r$, where $R = \mathcal{O}(1)$, and a scaled stream function $\psi = \mathcal{E}^{-1} \Omega$, where $\psi = \mathcal{O}(1)$. This allows one to formally separate the behavior in the far regime $\mathcal{E} \rightarrow 0$ (see Section 3) and the near regime $\mathcal{E} \rightarrow \infty$ (see Section 4). It is helpful to express the momentum equation and boundary conditions in terms of the scaled variables:

$$\nabla \times \nabla \cdot \left[(1 + \mathcal{E}^2 \dot{\boldsymbol{\gamma}}^2)^{\frac{n-1}{2}} \dot{\boldsymbol{\gamma}} \right] = 0, \quad (11)$$

$$\begin{aligned} \psi = 0, \quad \frac{1}{R} \frac{\partial \psi}{\partial \theta} = 1, \quad \text{on } \theta = 0, \\ \psi = 0, \quad \frac{\partial \psi}{\partial \theta} = 0, \quad \text{on } \theta = \alpha, \end{aligned} \quad (12)$$

where the shear-rate and rate of strain tensor are now expressed in terms of ψ and R . We will proceed by first analyzing the far corner region in Section 3.

3. The far corner approximation $\mathcal{E} \ll 1$

We seek a solution in the form of a regular perturbation series

$$\psi \sim \psi_0 + \mathcal{E}^2\psi_1 + \mathcal{E}^4\psi_2 + \dots \tag{13}$$

in the limit as $\mathcal{E} \rightarrow 0$. In this limit, the natural expansion of the viscosity is given by

$$[1 + \mathcal{E}^2\dot{\gamma}^2]^{\frac{n-1}{2}} \sim 1 + \left(\frac{n-1}{2}\right)\dot{\gamma}^2\mathcal{E}^2 + \frac{1}{2}\left(\frac{n-1}{2}\right)\left(\frac{n-3}{2}\right)\dot{\gamma}^4\mathcal{E}^4 + \mathcal{O}(\mathcal{E}^6). \tag{14}$$

Substituting the expansion for the viscosity into the momentum Eq. (7) and imposing the boundary conditions (10) one can see that the zeroth order term reduces to the Newtonian system, which is given by the biharmonic equation. The solution is given [16] as

$$\psi_0 = -R(B \sin(\theta) + C\theta \cos(\theta) + D\theta \sin(\theta)), \tag{15}$$

where B, C, D are constants given by

$$B = \frac{-\alpha^2}{\alpha^2 - \sin^2(\alpha)}, \quad C = \frac{\sin^2(\alpha)}{\alpha^2 - \sin^2(\alpha)}, \quad D = \frac{\alpha - \sin(\alpha)\cos(\alpha)}{\alpha^2 - \sin^2(\alpha)}. \tag{16}$$

Proceeding to $\mathcal{O}(\mathcal{E})$ the momentum equation can be written as

$$\nabla^4\psi_1 = \kappa \nabla \times \nabla \cdot (\dot{\gamma}_0^2 \dot{\gamma}_0), \tag{17}$$

where $\kappa_1 = \frac{n-1}{2}$, $\dot{\gamma}_0$ and $\dot{\gamma}_0$ are the zeroth order terms of the shear rate and rate of deformation tensor, given by $\dot{\gamma}_0 = 2R^{-2}(C \sin(\theta) - D \cos(\theta))$, $\dot{\gamma}_0 = \dot{\gamma}_0(\mathbf{e}_r \mathbf{e}_\theta + \mathbf{e}_\theta \mathbf{e}_r)$, where $\mathbf{e}_r, \mathbf{e}_\theta$ are unit vectors in the r, θ directions. Eq. (17) can now be expressed as

$$\nabla^4\psi_1 = 8\kappa_1 R^{-5} \left\{ \frac{\partial^2}{\partial \theta^2} [(C \sin \theta - D \cos \theta)^3] - 3(C \sin \theta - D \cos \theta)^3 \right\}. \tag{18}$$

For ψ_1 to have consistent dimensions, we seek a solution in the form $\psi_1 = R^{-1}f_1(\theta)$. Thus (18) reduces to

$$f_1^{iv} + 10f_1'' + 9f_1 = 8\kappa_1 \left\{ \frac{\partial^2}{\partial \theta^2} [(C \sin \theta - D \cos \theta)^3] - 3(C \sin \theta - D \cos \theta)^3 \right\}, \tag{19}$$

subject to the boundary conditions $f(0) = f'(0) = f(\alpha) = f'(\alpha) = 0$. Eq. (19) can be solved analytically for f_1 and leads to the expression

$$\psi_1 = R^{-1}\{(A_1 + B_1\theta)\cos(3\theta) + (C_1 + D_1\theta)\sin 3\theta + (E_1 + F_1\theta)\cos \theta + (G_1 + H_1\theta)\sin \theta\}, \tag{20}$$

where

$$B_1 = \frac{1}{2}(C^3 - 3CD^2)\kappa_1, \quad D_1 = \frac{1}{2}(3DC^2 - D^3)\kappa_1, \\ F_1 = \frac{3}{2}(C^3 + D^2C)\kappa_1, \quad H_1 = \frac{3}{2}(D^3 + DC^2)\kappa_1. \tag{21}$$

The constants A_1, C_1, E_1, G_1 are then derived from the boundary conditions. For simplicity, we give the result for the case $\alpha = \pi/2$, for which

$$\psi_1 = \frac{\kappa_1}{R(\pi^2 - 4)^3} \left\{ (8\pi^3 - 8(3\pi^2 - 4)\theta)\cos(3\theta) + (2(\pi^4 - 16) - 4\pi(\pi^2 - 12)\theta)\sin(3\theta) + (-8\pi^3 + 24(\pi^2 + 4)\theta)\cos \theta + (-2(3\pi^4 + 16) + 12(\pi^2 + 4)\theta)\sin \theta \right\}. \tag{22}$$

Proceeding to find the second order contribution leads to the partial differential equation

$$\nabla^4\psi_2 = \nabla \times \nabla \cdot [\kappa_1\dot{\gamma}_1^2\dot{\gamma}_0 + \kappa_1\dot{\gamma}_0^2\dot{\gamma}_1 + \kappa_2\dot{\gamma}_0^4\dot{\gamma}_0], \tag{23}$$

where $\kappa_2 = (n-1)(n-3)/8$, $\dot{\gamma}_1$, and $\dot{\gamma}_1$ are the $\mathcal{O}(\mathcal{E}^2)$ terms of the shear rate and rate of deformation tensor and can be expressed as

$$\dot{\gamma}_1^2 = 2R^{-4}(f_0'' + f_0)(f_1'' - 3f_1), \quad \dot{\gamma}_1 = R^{-3} \begin{pmatrix} -4f_1' & f_1'' - 3f_1 \\ f_1'' - 3f_1 & 4f_1' \end{pmatrix}, \tag{24}$$

respectively. We seek a solution in the form $\psi_2 = R^{-3}f_2(\theta)$, and the resulting ordinary differential equation (ODE) is

$$f_2^{iv}(\theta) + 34f_2'' + 225f_2 = N_1'' - 15N_1 - 8N_2'', \tag{25}$$

where

$$N_1 = 3\kappa(f_0'' + f_0)^2(f_1'' - 3f_1) + \kappa_2(f_0'' + f_0)^5, \quad N_2 = -4\kappa(f_0'' + f_0)^2f_1'. \tag{26}$$

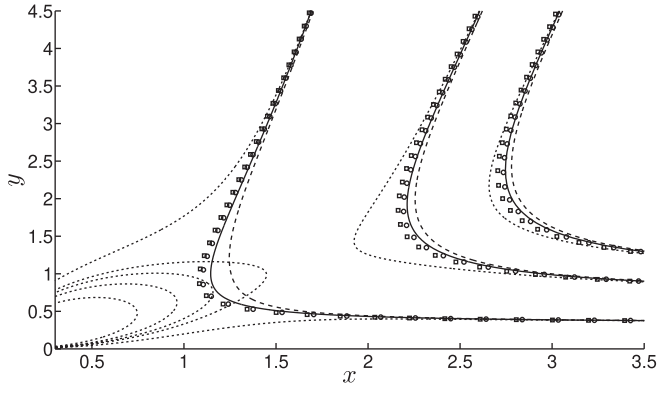
Eq. (25) could be solved analytically but as the solution is rather cumbersome we instead chose to solve it numerically to give $f_2(\theta)$. The series (13) is not uniformly convergent throughout the entire domain. If one considers the ratio of the first two terms, $\mathcal{E}^2\psi_1/\psi_0 \sim \mathcal{E}^2R^{-2}$, it can be seen that the assumption $\mathcal{E}^2\psi_1 \ll \psi_0$ fails when $R \sim \mathcal{E}$ (i.e. $r \sim \mathcal{O}(1)$). Physically, the loss of uniformity arises from the increase in shear rate as the apex of the corner is approached, thus the term $\mathcal{E}^2\dot{\gamma}^2$ becomes significant in the viscosity expansion (14). The solution is geometric in nature with R^{-2} acting analogous to a geometric ratio. Therefore, one might suspect that a rational fraction approximation might give a more uniform approximation. Applying Shanks transform, see [17] for further details, to the first three terms of the perturbation series and re-introducing the scaling for r, Ω we obtain the following approximation of the stream function:

$$\Omega_{\text{Shank}}(r, \theta) = r f_0' \left(\frac{f_0 f_1 - r^{-2}(f_2 f_0 - f_1^2)}{f_0 f_1 - r^{-2} f_2 f_0} \right). \tag{27}$$

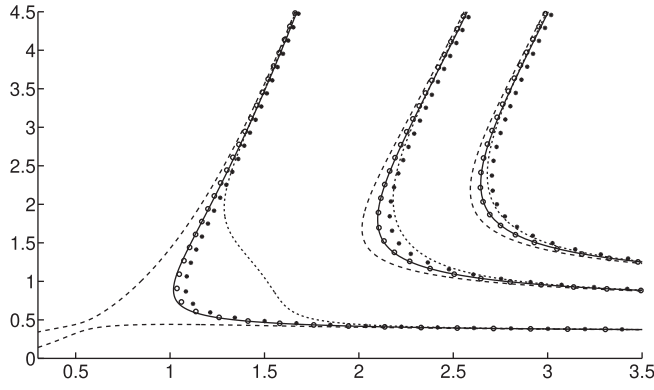
The streamlines are given in Fig. 2(a) for the case of a shear thinning fluid and Fig. 2(b) for a shear thickening fluid. The Newtonian solution is plotted together with the first and second order perturbation terms and the Shanks transform. To prove the validity of the expansion, Eqs. (2) and (3) are solved numerically using the finite element solver COMSOL Multiphysics. A Newtonian velocity field was imposed far from the corner with the moving and no-slip boundary conditions applied along the walls. Note that the first and second order terms quickly become invalid as the corner is approached, and thus only provide an appropriate correction from the zeroth order solution far from the corner. The Shanks transform improves convergence remarkably well for the shear thickening fluid even as the corner is approached, despite the underlying assumptions becoming invalid. However, for the shear thinning fluid, the Shanks transform does not perform as well. These results indicate that for shear thinning fluids the streamlines overshoot those of the Newtonian fluid, and that for shear-thickening fluids, the streamlines overshoot the Newtonian solution. A possible explanation for this is that as the viscosity of the system is reduced through shear thinning, the wall exerts a small shear stress on the fluid. A fluid element must be then closer to the moving wall before it can be dragged off horizontally.

4. Near corner approximation $\mathcal{E} \gg 1$

To further extend the domain in which analytic results can be found, we will now focus on the region closest to the corner where the shear rates are extremely large. We now consider the asymptotic series as $\mathcal{E} \rightarrow \infty$. As we expect the leading order behavior to be the power-law solution, the appropriate series expansions for the stream function and viscosity are



(a)



(b)

Fig. 2. A plot of the streamlines for (a) $n = 0.5$ and (b) $n = 1.7$, with a corner angle of $\alpha = \frac{\pi}{2}$. The first and second order perturbation solutions are given by the dashed and dotted–dashed lines, respectively. The exact numerical solution is denoted by the solid black line with the open circles and solid circles denoting the Shanks and Newtonian solutions, respectively.

$$\psi \sim \psi_0 + \mathcal{E}^{-2}\psi_1 + \mathcal{E}^{-4}\psi_2 + \dots \quad (28)$$

and

$$[1 + \mathcal{E}^2\dot{\gamma}^2]^{\frac{n-1}{2}} \sim \mathcal{E}^{n-1}\dot{\gamma}^{n-1} + \kappa_1 \mathcal{E}^{n-3}\dot{\gamma}^{n-3} + \dots \quad (29)$$

Comparing orders of \mathcal{E} , the momentum equation gives

$$\nabla \times \nabla \cdot \{\dot{\gamma}_0^{n-1} \dot{\gamma}_0\} = \mathbf{0} \quad \text{at order } \mathcal{O}(\mathcal{E}^{n-1}), \quad (30)$$

$$\nabla \times \nabla \cdot \{(n-1)\dot{\gamma}_1 \dot{\gamma}_0^{n-2} \dot{\gamma}_0 + \dot{\gamma}_0^{n-1} \dot{\gamma}_1 + \kappa_1 \dot{\gamma}_0^{n-3} \dot{\gamma}_0\} = \mathbf{0} \quad \text{at order } \mathcal{O}(\mathcal{E}^{n-3}). \quad (31)$$

The zeroth order solution, ψ_0 , was obtained previously by Riedlerand Schneider [12], where $\psi_0 = Rg_0(\theta)$ and g_0 is given by the expression

$$g_0(\theta) = \left(1 - \frac{K_1(\theta)}{K_1(\alpha)}\right) \sin \theta + \frac{K_2(\theta)}{K_1(\alpha)} \cos \theta, \quad (32)$$

where

$$K_1(\theta) = \int_0^\theta |F(\theta')|^{\frac{1}{n}} \cos(\theta') d\theta', \quad K_2(\theta) = \int_0^\theta |F(\theta')|^{\frac{1}{n}} \sin(\theta') d\theta', \quad (33)$$

with

$$F(\theta) = \begin{cases} \sin(\sqrt{n(2-n)}(\theta - \theta_\infty)) & \text{for } n < 2, \\ \sqrt{(\theta - \theta_\infty)} & \text{for } n = 2, \\ \sinh(\sqrt{n(n-2)}(\theta - \theta_\infty)) & \text{for } n > 2. \end{cases} \quad (34)$$

The parameter θ_∞ is found by requiring that $K_2(\alpha) = 0$. The solution for g_0 can be obtained from analysis of the momentum equation which reduces to

$$n(n-2)|g_0 + g_0''|^{n-1}(g_0 + g_0'') = [|g_0 + g_0''|^{n-1}(g_0 + g_0'')]', \quad (35)$$

where $'$ denotes differentiation with respect to θ . The solution for $g_0 + g_0''$ gives

$$\text{sgn}(g_0 + g_0'') |g_0 + g_0''|^n = \begin{cases} A \sin(\sqrt{n(2-n)}(\theta - \theta_\infty)) & \text{for } n < 2, \\ A(\theta - \theta_\infty) & \text{for } n = 2, \\ A \sinh(\sqrt{n(n-2)}(\theta - \theta_\infty)) & \text{for } n > 2, \end{cases} \quad (36)$$

where $A^{-\frac{1}{n}} = K_1(\alpha) |n(n-2)|^{\frac{1}{2n}}$. Eqs. (32) and (33) can then be obtained by the method of variation of parameters and applying the constraints $g_0(0) = g_0(\alpha) = g_0'(\alpha) = 0$ and $g_0'(0) = 1$. We will now focus on the perturbed partial differential equation (PDE) (31). On dimensional grounds we will seek a solution of the form $\psi_1 = R^3 g_1(\theta)$. One can examine the region where the series is valid prior to the calculation of g_1 . If one assumes g_1 is $\mathcal{O}(1)$, and that ψ_0 and ψ_1 increase as R and R^3 , respectively, then the first order solution loses its uniformity again when $\frac{\psi_0}{\mathcal{E}^{-2}\psi_1}$ is $\mathcal{O}(1)$, i.e. when R is $\mathcal{O}(\mathcal{E}^{-1})$. This corresponds to the same region as that where the Newtonian solution loses uniformity. In effect, we have sandwiched the region of non-uniformity from above and from below. The zeroth and first order terms for the shear rate and rate of strain tensors can be written as

$$\dot{\gamma}_0 = R^{-1}|g_0 + g_0''|, \quad \dot{\gamma}_0 = R^{-1} \begin{pmatrix} 0 & g_0 + g_0'' \\ g_0 + g_0'' & 0 \end{pmatrix}, \\ \dot{\gamma}_1 = R \cdot \text{sgn}\{(g_0'' + g_0)\} \cdot (g_1'' - 3g_1), \quad \dot{\gamma}_1 = R \begin{pmatrix} 4g_1' & g_1'' - 3g_1 \\ g_1'' - 3g_1 & -4g_1' \end{pmatrix}. \quad (37)$$

Substituting (37) into the 1st order momentum Eq. (31) leads to the ODE

$$-\frac{d^2}{d\theta^2} \{n|g_0 + g_0''|^{n-1}(g_1'' - 3g_1) + \kappa_p |g_0 + g_0''|^{n-2}\} \\ + 8(n-3) \frac{d}{d\theta} \{|g_0 + g_0''|^{n-1} g_1'\} \\ + (n-2)(n-4) \{n|g_0 + g_0''|^{n-1}(g_1'' - 3g_1) + \kappa_p |g_0 + g_0''|^{n-2}\} = 0, \quad (38)$$

where

$$\kappa_p = \text{sgn}\{(g_0'' + g_0)\} \kappa. \quad (39)$$

g_1 is subject to the homogeneous conditions

$$g_1(0) = g_1'(0) = g_1(\alpha) = g_1'(\alpha) = 0. \quad (40)$$

Eq. (38) has a regular singular point when $g_0 + g_0'' = 0$. From Eq. (36), it can be seen that this occurs when $\theta = \theta_\infty$. We now shift the coordinate system so that $\theta = \theta_\infty$ maps to $\theta = 0$. One would expect difficulties to arise in the formulation as $\dot{\gamma} \rightarrow 0$, as the expansion for the viscosity (29) will clearly fail. This problem is rectified in Section 5. As no exact closed form analytical solution to Eq. (38) can be found except for special parameter choices (see Appendix A), we proceed by seeking the homogeneous solution to (38). To find the general solution we will seek a series in the form

$$g_1(\theta) = \sum_{i=0}^{\infty} \hat{g}_i(\theta)^{i+\beta}, \quad (41)$$

and use the series expansion

$$g_0 + g_0'' \sim \mathcal{A} \operatorname{sgn}(K_1(\alpha)\theta) |\theta|^{\frac{1}{n}} \left[1 + \frac{(n-2)}{6} \theta^2 - \frac{(n-2)^2(2n-5)}{360} \theta^4 \right] + \mathcal{O}\left(\theta^{6+\frac{1}{n}}\right) \text{ for } n \neq 2, \tag{42}$$

which is obtained from Eq. (36) and we define $\mathcal{A} = |K_1(\alpha)|^{-1} n^{\frac{1}{2n}} |2-n|^{\frac{1}{2n}}$. Substituting the series (41) and (42) into (38), it is seen that for a non-trivial series expansion β must satisfy

$$\beta(\beta-1)(n\beta-(n+1))(n\beta-(2n+1)) = 0. \tag{43}$$

The roots of (43) allow one to construct the four linearly independent solutions which can be written for $\frac{1}{n} \notin \mathbb{N}$ as

$$\begin{aligned} k_1 &\sim 1 + \frac{3}{2}\theta^2 + \frac{25n-51}{8(3n-1)}\theta^4 + \dots, \\ k_2 &\sim \theta \left(1 + \frac{1}{6} \frac{(14n-27)}{(2n-1)}\theta^2 - \frac{128n^4-2136n^3+7258n^2-8001n+2025}{120(2n-1)(3n-1)(4n-1)}\theta^4 + \dots \right), \\ k_3 &\sim \theta^{1+\frac{1}{n}} \left(1 + \frac{1}{2} \frac{(n-2)(2n^2+33n+25)}{(2n+1)(3n+1)}\theta^2 - \frac{(n-2)(48n^6-116n^5+220n^4-18095n^3+11362n^2+31171n+8170)}{360(2n+1)(3n+1)(4n+1)(5n+1)}\theta^4 + \dots \right), \\ k_4 &\sim \theta^{2+\frac{1}{n}} \left(1 - \frac{6n^3-53n^2+65n+42}{6(3n+1)(4n+1)}\theta^2 + \frac{336n^7-716n^6-6516n^5+47975n^4-93312n^3+16385n^2+11380}{360(2n+1)(3n+1)(4n+1)(5n+1)(6n+1)}\theta^4 + \dots \right). \end{aligned} \tag{44}$$

The homogeneous solution is unphysical for $\theta < 0$ as for certain values of n the solution may be complex, moreover, the functions k_3 and k_4 are never smooth at the point $\theta = 0$. The way to overcome this is by separating the solution into two domains for $\theta > 0$ and $\theta < 0$, and then matching the solution across the boundary $\theta = 0$. The homogeneous equation, obtained by setting $\kappa_p = 0$ in Eq. (38), is invariant under the transformation $\theta \rightarrow -\theta$. We thus separate the solution into

$$g_{\text{homo}} = \begin{cases} A^+ k_1(\theta) + B^+ k_2(\theta) + C^+ k_3(\theta) + D^+ k_4(\theta) & \theta > 0, \\ A^- k_1(-\theta) + B^- k_2(-\theta) + C^- k_3(-\theta) + D^- k_4(-\theta) & \theta < 0. \end{cases} \tag{45}$$

We later show that $A^+ = A^-$, $B^+ = -B^-$, $C^+ = C^-$ and $D^+ = -D^-$. The inhomogeneous solution can again be found by seeking a Frobenius series solution given by

$$k_p = \operatorname{sgn}(\theta) \mathcal{A}^{-1} \theta^{2-\frac{1}{n}} \left(-\frac{n}{2(2n-1)} - \frac{(12n^4-60n^3+187n^2-81n+2)n(n-2)}{12(4n-1)(3n-1)(3n-2)(2n-1)} \theta^2 + \dots \right). \tag{46}$$

Note that the singularity at $n = 2$ arises as a result of the change of behavior of the zeroth order solution and must be considered separately. The singularities at $n = \frac{1}{2}$ in the first term and $n = \frac{1}{4}, \frac{1}{3}, \frac{3}{2}$ in the second term can be resolved using by the introduction of logarithmic terms [18]. Eq. (46) gives the complete outer-solution, however, for matching across the boundary we need only consider the limit as $\theta \rightarrow 0$. The leading order behavior could be found more directly without the need to obtain the full solution (see Appendix B). Evaluation of either method results in the expression

$$\psi_1 \sim \begin{cases} -\frac{n}{2(2n-1)} K_1(\alpha) \left(n^{\frac{1}{2n}} (n-2)^{\frac{1}{2n}} \right)^{-1} R^3 \theta^{2-\frac{1}{n}} & \text{as } \theta \rightarrow 0^+, \\ + \text{homogeneous terms} \\ \frac{n}{2(2n-1)} K_1(\alpha) \left(n^{\frac{1}{2n}} (n-2)^{\frac{1}{2n}} \right)^{-1} R^3 (-\theta)^{2-\frac{1}{n}} & \text{as } \theta \rightarrow 0^-. \\ + \text{homogeneous terms} \end{cases} \tag{47}$$

The asymptotic behavior of g_0 as $\theta \rightarrow 0$ can be found by solving (42) and keeping the first term on the left hand side of the series. The equation can be integrated to give a solution which can be written in terms of hyper-geometric functions. However, for the case of $\frac{1}{n} \notin \mathbb{N}$, if

we take the leading order term in the Taylor series we find

$$g_0^\pm \sim \sin(\theta + \theta_\infty) + C_0^\pm \left((\pm\theta)^{2+\frac{1}{n}} + \dots \right), \text{ as } \theta \rightarrow \pm 0, \tag{48}$$

where the first term, which arises from the homogeneous term in Eq. (36), does not contribute to the shear rate and C_0^\pm is given by

$$C_0^\pm = \pm \frac{\mathcal{A} n^2 \operatorname{sgn}(K_1(\alpha))}{(2n+1)(n+1)}. \tag{49}$$

We can see that the stream function ψ behaves as $\mathcal{O}(1)$ where the first order term has fractional powers of $\theta^{1+\frac{1}{n}}$, $\theta^{2-\frac{1}{n}}$. The stream function is uniformly valid if $\theta \rightarrow 0$ for $2 - \frac{1}{n} > 0$. However, the shear rate and thus the stress tensor, are not uniformly valid for any $n > 0$. It is clear that the solution breaks down along the line $\theta = 0$ due to the shift from power law to Newtonian behavior. To analyze this change in physical behavior we assume that a boundary layer of unknown thickness exists around $\theta = 0$. We adopt Cartesian variables as polar coordinates offer no advantage, and we use the approach proposed by Renardy [19]. We chose our Cartesian system such that x, y are parallel and perpendicular to the line $\theta = 0$ respectively (Fig. 3).¹ Let us now suppose that the boundary layer has thickness δ which leads to the introduction of the scalings $y = \delta Y$, $x = X$. Note that the polar coordinates are related to the Cartesian coordinates by $R \sim X$, $\theta \sim \delta Y/X$, which will be used later in the matching process. In the inner boundary layer, the scaling of the stream function remains unknown, and we adopt an arbitrary scaling

$$\psi_{\text{inner}} = \Delta_0 \Psi + g(0)X + \delta g'(0)Y, \tag{50}$$

where X, Y and Ψ are $\mathcal{O}(1)$ and the orders of δ and Δ_0 remain to be determined. The last two terms in Eq. (50) are included to account for the homogeneous term in Eq. (48). Physically these terms represent a constant velocity flowing into the boundary layer, but have no effect on the momentum equation. Under these scalings it useful to note that the velocity gradients are given by

$$u_x = -v_y = -\Delta_0 \delta^{-1} \Psi_{XY}, v_x = \Delta_0 \Psi_{XX}, u_y = -\Delta_0 \delta^{-2} \Psi_{YY}. \tag{51}$$

Physically the X derivatives should be small compared to the Y derivatives as no change in the velocity gradients occurs in the outer solution in this direction. In Cartesian variables, the momentum Eq. (7) can be written as

$$\left(\frac{\partial^2}{\partial x^2} - \frac{\partial^2}{\partial y^2} \right) \tau_{xy} + \frac{\partial^2}{\partial x \partial y} (\tau_{yy} - \tau_{xx}) = 0. \tag{52}$$

Substituting (50) into (7) and keeping the lowest order terms, one finds

$$\nabla \times \nabla \cdot \left\{ \left(1 + \mathcal{E}^2 \Delta_0^2 \delta^{-4} \Psi_{YY}^2 \right)^{\frac{n-1}{2}} \Delta_0 \delta^{-2} \Psi_{YY} \mathbf{e}_x \mathbf{e}_y \right\} = \mathbf{0}. \tag{53}$$

We now argue that within this layer there must be a transition between Newtonian and non-Newtonian behavior. In the power-law region, the shear-dependent term $\mathcal{E}^2 \dot{\gamma}^2$ dominates the $+1$ term in the viscous Eq. (1), and likewise in the Newtonian case the $+1$ term dominates over the shear term, thus for a transition to occur we require that they are both of the same order. Hence $\mathcal{E} \Delta_0 \delta^{-2}$ must be $\mathcal{O}(1)$, giving the first condition, $\Delta_0 = \mathcal{E}^{-1} \delta^2$. Substituting for Y and keeping the leading order terms gives

$$\left[\left(1 + \Psi_{YY}^2 \right)^{\frac{n-1}{2}} \Psi_{YY} \right]_{YY} = 0, \tag{54}$$

which we will refer to throughout as “the boundary layer equation”. We can readily see that this PDE permits similarity solutions of the form

$$\Psi = X^b \phi \left(X^{-\frac{b}{2}} Y \right). \tag{55}$$

The constant b is determined by requiring that the inner solution must match up to the outer solution $\psi = R \theta^{2+\frac{1}{n}} \sim \delta^{2+\frac{1}{n}} X^{-(1+\frac{1}{n})} Y^{2+\frac{1}{n}}$. This

¹ We assume that x, y are of the same order of R and not r , i.e. $R^2 = x^2 + y^2$.

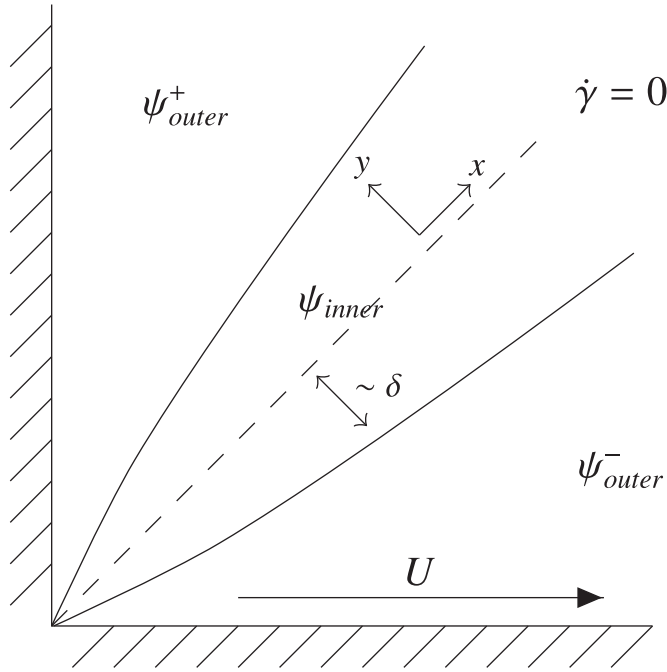


Fig. 3. Sketch of boundary layer system for $\alpha = \frac{\pi}{2}$.

requires that $b - \frac{b}{2}(2 + \frac{1}{n}) = -(1 + \frac{1}{n})$, which leads to $b = 2 + 2n$. The boundary layer equation subsequently becomes

$$\Psi = X^{2+2n}\phi(\chi), \quad \left[(1 + \phi^{n2})^{\frac{n-1}{2}} \phi'' \right]' = 0, \quad (56)$$

where ' denotes differentiation with respect to χ , with $\chi = X^{-(1+n)}Y$. This matching condition is satisfied if $\phi \sim \chi^{2+\frac{1}{n}}$ as $\chi \rightarrow \infty$. Integrating twice and setting the constant term to be zero we obtain the non-linear second order ODE

$$[1 + \phi^{n2}]^{\frac{n-1}{2}} \phi'' = A_b \chi. \quad (57)$$

Though no general closed form solution to Eq. (57) can be found, the asymptotic behavior can be readily seen. First let us consider the case as $\chi \rightarrow \infty$, whereby the left-hand side of (57) must become large. This requires ϕ'' to become large and thus the + 1 term becomes negligible, hence $[1 + \phi^{n2}]^{\frac{n-1}{2}} \phi'' \approx (\phi^n)^n$. Thus $\phi'' \sim \chi^{\frac{1}{n}}$ as $\chi \rightarrow \infty$ and hence $\phi \sim \chi^{\frac{1}{n}+2}$, which is the correct matching condition. For the inner solution as $\chi \rightarrow 0$ the left-hand side of Eq. (57) must be small and thus $\phi'' \ll 1$. Hence $[1 + \phi^{n2}]^{\frac{n-1}{2}} \phi'' \approx \phi''$. Thus, the inner behavior is as $\phi \sim \chi^3$. We can see the change in behavior by solving the boundary layer equation $(1 + \phi^{n2})^{\frac{n-1}{2}} \phi'' = \chi$ numerically. This was achieved by integrating $\phi'' = Z(x)$ using a second order finite difference scheme, where $Z(x)$ is the inverse function of $P(x) = (1 + x^2)^{\frac{(n-1)}{2}}x$, which was found using the Newton Raphson method. The solution is shown in Fig. 4, along with the inner and outer approximations. This permits us to examine the boundary layer behavior as the Newtonian limit is approached. If the fluid is everywhere Newtonian, there is no change in behavior and thus there must be no boundary layer. One might have expected that the size of the layer would tend to zero, however, we find its size in fact tends to ϵ^{-1} . In the Newtonian limit, we actually find the inner behavior χ^3 , and the outer behavior $\chi^{2+\frac{1}{n}}$, coincide and thus no change in behavior occurs.

We can now see that behavior of the inner solution far from the boundary can be written in terms of the outer variables x, y as

$$\psi_{inner} \sim \Delta_0 X^{-(1+\frac{1}{n})} Y^{2+\frac{1}{n}} = \Delta_0 \delta^{-(2+\frac{1}{n})} \chi^{-(1+\frac{1}{n})} y^{2+\frac{1}{n}}. \quad (58)$$

Thus, for the orders to match, we require that $\Delta_0 = \delta^{(2+\frac{1}{n})}$. By

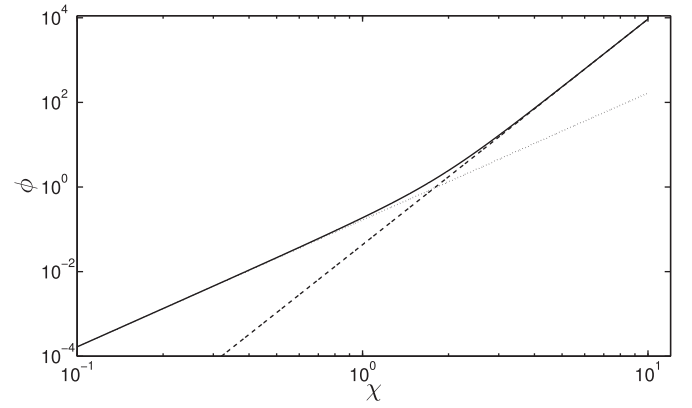


Fig. 4. Solution for $(1 + \phi^{n2})^{\frac{n-1}{2}} \phi'' = \chi$ given by the solid line with the inner, χ^3 , and outer, $\chi^{2+\frac{1}{n}}$, behaviors given by the dotted and dashed lines, respectively, for the case of $n = \frac{3}{10}$.

combining this with the first condition, $\Delta_0 = \epsilon^{-1}\delta^2$, we get the explicit scaling of the boundary layer $\delta = \epsilon^{-n}$ and $\Delta_0 = \epsilon^{-(2n+1)}$. Physically, we see that this new scaling is applicable when $\epsilon \sim \dot{\gamma}^{-1}$ as to be expected.

This scaling could alternatively have been deduced from looking at the form of the behavior of the outer solution. The behavior of the zeroth order term it is as $r\theta^{2+\frac{1}{n}}$ and for the first order term it is as $\epsilon^{-2}R^3\theta^{2-\frac{1}{n}}$ for $n < 2$. By considering the ratio of these terms we see that the solution loses its uniformity when

$$\frac{R\theta^{2+\frac{1}{n}}}{\epsilon^{-2}R^3\theta^{2-\frac{1}{n}}} = (\epsilon^n R^{-n} \theta)^{\frac{2}{n}} = \mathcal{O}(1). \quad (59)$$

As we consider R to be $\mathcal{O}(1)$ this gives the required scaling for θ as $\mathcal{O}(\epsilon^{-n})$. The scaling for ψ becomes apparent whilst expressing the first term in the outer series in terms of the scaled θ , i.e. if $\theta = \epsilon^{-n}\Theta$, then $\psi_0 = R\epsilon^{-(2n+1)}\Theta^{2+\frac{1}{n}}$. Likewise, one can see that the similarity variable appears as the ratio of the power-law and viscous correction terms. In Section 5, we will formally match the boundary layer equation to the outer solution.

The boundary layer occurs when $Y \sim \epsilon^{-n}$. The scaling suggests that as n grows large this boundary layer region becomes infinitely small, with the inner stream function scaling also becoming smaller, though we later find that for asymmetric flows an additional layer of width ϵ^{-2} occurs which dominates for $n > 2$. This is discussed in Section 5.3. However, as most fluids exhibit shear thinning properties, often $n < 1$ and consequently this layer would be much smaller than the ϵ^{-n} layer.

5. Matching

5.1. Leading order

As two of the boundary conditions are applied in the region $\theta > 0$, and the other two in the region $\theta < 0$, to get a complete solution we must match the solutions over the boundary layer. We first consider the case of $n < 2$. The case of $n > 2$ is considered in Section 5.3. The free parameters of the outer solution (47) can be matched to the inner solution to obtain a solution defined across the whole domain. As the inner scaling can be derived from consideration of where the outer shear rate loses its uniformity, this suggests that the zeroth and first order terms in the outer series match to the lowest order in the inner series. We now formally match the leading order inner solution to the outer solutions. Considering the expansion for the outer solution (57) and using the series approximation for large ϕ'' , we obtain

$$\left| \phi'' \right|^{n-1} \phi'' + \frac{n-1}{2} |\phi''|^{n-3} \phi'' + \dots = A_p \chi. \quad (60)$$

We can construct the inverse series, by means of iteration, to find

$$\phi'' = f(\chi) \sim \sum_{m=0}^{\infty} \beta_m \chi^{\frac{1}{n} - \frac{2m}{n}} \sim \text{sgn}(A_p \chi) \left\{ (|A_p \chi|)^{\frac{1}{n}} - \frac{n-1}{2n} (|A_p \chi|)^{-\frac{1}{n}} \right\} + \mathcal{O}\left(\chi^{-\frac{3}{n}}\right), \tag{61}$$

which integrates to give

$$\phi = A + B\chi + \int_0^\chi \int_0^{\chi'} f(\chi'') d\chi'' d\chi' \sim (A + Int_1) + (B + Int_2)\chi + \tag{62}$$

$$\frac{\text{sgn}(\chi)n^2}{(n+1)(2n+1)} \text{sgn}(A_p) \left| A_p \right|^{\frac{1}{n}} |\chi|^{2+\frac{1}{n}} - \frac{\text{sgn}(\chi)n}{2(2n-1)} \text{sgn}(A_p) \left| A_p \right|^{\frac{1}{n}} |\chi|^{2-\frac{1}{n}} + \dots \text{ as } \chi \rightarrow \infty, \tag{63}$$

where Int_1, Int_2 are the order 1 contributions which arise from the contribution to the integral for χ not large. These are calculated numerically by

$$Int_2 = \int_0^\infty (f(\chi') - \text{sgn}(A_p \chi') (|A_p \chi'|)^{\frac{1}{n}}) d\chi', \tag{64}$$

$$Int_1 = \int_0^\infty \left(\int_0^{\chi'} f(\chi'') d\chi'' - \sum_{m=0}^{1+\frac{1}{n}-\frac{2m}{n}<0} \frac{\beta_m}{\left(1+\frac{1}{n}-\frac{2m}{n}\right)} \chi^{1+\frac{1}{n}-\frac{2m}{n}} - Int_2 \right) d\chi'. \tag{65}$$

Via Van Dyke’s matching rule [20] if $A = -Int_1, B = -Int_2$ and $\text{sgn}(A_p) |A_p|^{\frac{1}{n}} = K_1(\alpha)^{-1} n^{\frac{1}{2n}} (n-2)^{\frac{1}{2n}}$, or equivalently $A_p = \text{sgn}(K_1(\alpha)) |K_1(\alpha)^{-n} n^{\frac{1}{2}} (n-2)^{\frac{1}{2}}|$, and as $\text{sgn}(\theta) = \text{sgn}(\chi)$, then the outer limit of ϕ is given by

$$\phi = \frac{n^2 \text{sgn}(\theta) K_1(\alpha)^{-1} n^{\frac{1}{2n}} (n-2)^{\frac{1}{2n}}}{(n+1)(2n+1)} |\chi|^{2+\frac{1}{n}} - \frac{\text{sgn}(\theta)n}{2(2n-1)} K_1(\alpha) \left(n^{\frac{1}{2n}} (n-2)^{\frac{1}{2n}} \right)^{-1} |\chi|^{2-\frac{1}{n}} + \dots, \tag{66}$$

which matches exactly with the inner behavior of the inhomogeneous terms in the outer solution obtained previously (47) and (48). Reverting back to polar coordinates and introducing the scaling for r, Ω allows one to incorporate the Newtonian effects to leading order from use of the composite approximation to zeroth order with the expression

$$\Omega_{\text{comp}} = r \left(g_0(\theta) - C^+ |\theta|^{2+\frac{1}{n}} \text{sgn}(\theta) \right) + r^{2+2n} \phi(r^{-n}\theta). \tag{67}$$

The composite expansion gives an expression that is uniformly valid over the troublesome zero shear layer (Fig. 5), though it is important to note that it does not resolve the loss of uniformity due to the radial decrease in shear rate. The composite streamlines are plotted in Fig. 6 along with the power-law solution and complete numerical solution for a Carreau fluid as with Fig. 2. One can see that the first order solution correctly captures the behavior of the Carreau fluid for small r , although the loss of uniformity is apparent as the radial distance grows.

5.2. Matching homogeneous terms: second internal boundary layer

To correctly apply the boundary conditions the constants A^+, B^+, C^+, D^+ must be matched to the corresponding terms in the lower domain, A^-, B^-, C^-, D^- . Using the aforementioned scaling leads one to look for an inner solution of the form

$$\psi_{\text{inner}} = \sin(\theta_\infty)X + e^{-n} \cos(\theta_\infty)Y + e^{-(2n+1)}X^{2+2n}\phi + e^{-2}\Psi_A + e^{-(n+2)}\Psi_B + e^{-(n+3)}\Psi_C + e^{-(2n+3)}\Psi_D, \tag{68}$$

where $\Psi_A, \Psi_B, \Psi_C, \Psi_D$ map to k_1, k_2, k_3, k_4 , respectively. The details are

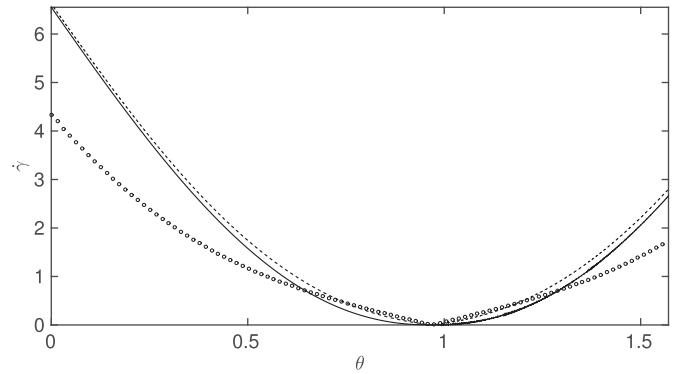


Fig. 5. The shear rate along the contour $r = 1$ for $n = 0.45, \alpha = \frac{\pi}{2}$ is plotted. The outer power-law solution (solid line), the inner boundary solution (circular markers) and the composite curve (dashed lines) are shown.

given in [18]. After matching to the outer solutions the inner shear-rate is found to have inner behavior

$$\Psi_{YY} = e^{-(2n+1)}A_b X^{-(1+n)}Y + e^{-(n+3)}\frac{(n+3)}{n^2}C^+ X^{2-\frac{1}{n}} + e^{-(2n+3)}D^+ \frac{(n+1)(2n+1)}{n^2}X^{1-\frac{1}{n}}Y.$$

The leading order shear rate behaves as $e^{-(2n+1)}Y$, whereas the homogeneous terms give rise to a shear rate $e^{-(n+3)}$. This results in a loss of uniformity when $Y \sim e^{n-2}$ which arises because the point of zero shear no longer occurs when $Y = 0$ as predicted by the pure power-law solution. Instead, the point of zero shear has been shifted due to the presence of the anti-symmetric flow term. Physically this is to be expected as one would not anticipate a Carreau fluid to have exactly the same point of zero shear as a pure power-law fluid.

This leads us to propose a second inner scaling whereby $Y = e^{n-2}\mathcal{Y}$, which can be written as $y = e^{-2}\mathcal{Y}$ in terms of the outer coordinates. This scaling describes purely Newtonian behavior and does not change so one can simply express (68) in terms of this scaling. The solution can therefore be written as

$$\psi_{\text{inner}} = \sin(\theta_\infty)X + e^{-2}(A^+X^3 + \cos(\theta_\infty)\mathcal{Y}) + e^{-4}B^+X^2\mathcal{Y} + e^{n-7}\left(\frac{n+1}{2n}C^+X^{2-\frac{1}{n}}\mathcal{Y}^2 + X^{2+2n}\mathcal{Y}^3\right) + e^{n-9}\frac{(n+1)(2n+1)}{6n^2}X^{1-\frac{1}{n}}D^+\mathcal{Y}^3, \tag{69}$$

which leads to a uniformly valid shear-rate. By considering the limit as $Y \rightarrow 0^-$ in conjunction with symmetry arguments leads to the matching constraints $A^+ = A^-, B^+ = -B^-, C^+ = C^-$ and $D^+ = -D^-$. We now have a smooth uniform approximation, which completes the matching.

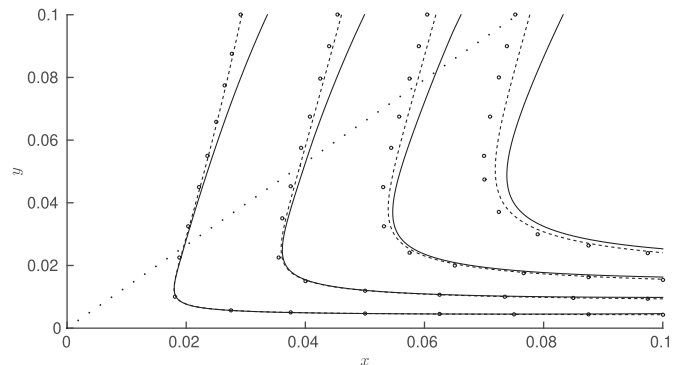


Fig. 6. The composite streamline (dashed lines) along with pure power-law solution (solid lines) and the numerical computed streamlines (circular markers) are shown. The line of zero shear is indicated by the dotted line.

The effect of the inner boundary layers is shown in Fig. 7, where the shear rate is plotted for fixed r . The effect of the second inner layer of shifting the point of zero shear can be observed.

5.3. Strong shear thickening fluids.

In the case of $n > 2$, the previous matching is no longer valid. This can be explained by considering the expression for the shear rate taking the first order terms in the outer series,

$$\dot{\gamma}_{\text{outer}} = C_0 R \theta^{\frac{1}{n}} + \mathcal{E}^{-2} R^3 \left(C^+ \theta^{-1+\frac{1}{n}} - \frac{n-1}{2n} \theta^{-\frac{1}{n}} + \mathcal{O}(1) \right). \quad (70)$$

The first term in the brackets arises from k_3 in the homogeneous solution (44), with the constant C^+ derived from the boundary conditions, and the second from the inhomogeneous term. For $n > 2$, as $\theta \rightarrow 0^+$, we see that the contribution from the homogeneous term is larger than that of the inhomogeneous term and the solution loses its uniformity before $y \sim \mathcal{E}^{-n}$. From analysis of the ratio of the two terms we propose an inner scaling of the form $y = \mathcal{E}^{-2} Y$, $\psi \sim \mathcal{E}^{-4-\frac{2}{n}} \hat{\Psi}$. This new scaling is required as the innermost boundary layer (of thickness \mathcal{E}^{-2}) is now larger than the previous outer layer (of thickness \mathcal{E}^{-n}). Upon using this scaling and keeping only the first order terms, the momentum equation reduces to

$$((\hat{\Psi}_{YY})^n)_{YY} = 0. \quad (71)$$

Integrating Eq. (71) gives

$$\hat{\Psi}_{YY} = (C_p^n Y + D_p)^{\frac{1}{n}} \sim \begin{cases} C_p Y^{\frac{1}{n}} + n^{-1} D_p C_p^{1-n} Y^{\frac{1}{n}-1} & \text{as } Y \rightarrow \infty, \\ D_p^{\frac{1}{n}} + n^{-1} D_p^{1-\frac{1}{n}} C_p^n Y & \text{as } Y \rightarrow 0, \end{cases} \quad (72)$$

where C_p and D_p can be functions of X . We can immediately see that the zero shear rate no longer occurs at $Y=0$. We now set $C_p = K_1(\alpha)^{-1} n^{\frac{1}{2n}} (n-2)^{\frac{1}{2n}} X^{-(1+\frac{1}{n})}$ and $D_p = n C_p^{n-1} C^+ X^{2-\frac{1}{n}}$ and match the other homogeneous solutions and the inhomogeneous term. Thus, we seek a solution of the form

$$\psi_{\text{inner}} = \sin(\theta_\infty) X + \mathcal{E}^{-2} \cos(\theta_\infty) Y + \mathcal{E}^{-4-\frac{2}{n}} \hat{\Psi} + \mathcal{E}^{-2} \hat{\Psi}_A + \mathcal{E}^{-4} \hat{\Psi}_B + \mathcal{E}^{-6-\frac{2}{n}} \hat{\Psi}_D + \mathcal{E}^{-6+\frac{2}{n}} \hat{\Psi}_I, \quad (73)$$

where $\hat{\Psi}_A$, $\hat{\Psi}_B$, and $\hat{\Psi}_D$ match to k_1 , k_2 and k_4 . We again set $\hat{\Psi}_A = A^+ X^3$ and $\hat{\Psi}_B = B^+ X^2 Y$ and note that $\hat{\Psi}_C$ is excluded as k_3 has already been matched in (72). The introduction of $\hat{\Psi}_I$ is required to match to the inhomogeneous term. The equations for $\hat{\Psi}_D$ and $\hat{\Psi}_I$ are given by

$$\left[\hat{\Psi}_{YY}^{n-1} \hat{\Psi}_I_{YY} + \frac{(n-1)}{2} \hat{\Psi}_{YY}^{n-2} (1 + 2\hat{\Psi}_{YY} \hat{\Psi}_I_{YY}) \right]_{YY} = 0, \quad (74)$$

$$[\hat{\Psi}_{YY}^{n-1} \hat{\Psi}_D_{YY}]_{YY} = 0. \quad (75)$$

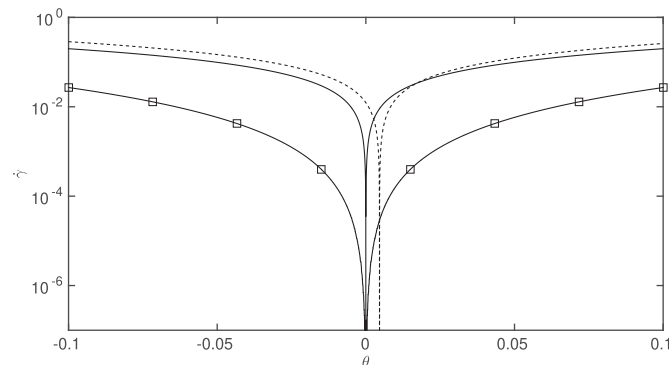


Fig. 7. The shear rate for the power-law fluid along $r = 1$, $n = 0.45$ is indicated by the line with the square markers. The solid line denotes the zeroth order composite solution and the dashed line represents the inclusion of the second inner layer.

The additional $+1$ term for Ψ_I results from expanding the term in the constitutive equation for viscosity, $1 + \mathcal{E}^2 \dot{\gamma}^2 \approx 1 + \mathcal{E}^2 (\psi_{\text{inner } YY})^2$. For Ψ_I the cross term is $\mathcal{O}(1)$, hence the inclusion of the $+1$ term in (74). If we again consider the limit as $Y \rightarrow \infty$, $\Psi_{YY} \sim C_p Y^{\frac{1}{n}}$, and Eq. (74) can be written as

$$\left[Y^{1-\frac{1}{n}} \hat{\Psi}_I_{YY} \right]_{YY} = \left[-\frac{(n-1)}{2n C_p} Y^{1-\frac{2}{n}} \right]_{YY}. \quad (76)$$

The inhomogeneous term gives rise to a particular solution

$$\hat{\Psi}_I = -\frac{n}{(2n-1)} K_1 n^{-\frac{1}{2n}} (n-2)^{-\frac{1}{2n}} X^{(1+\frac{1}{n})} Y^{2-\frac{1}{n}}, \quad (77)$$

which correctly maps to the outer solution. To obtain the inner solution behavior of (74), we note that $\hat{\Psi}_{YY} \sim D_p^{\frac{1}{n}}$ as $Y \rightarrow 0$, and thus

$$[\hat{\Psi}_I_{YY}]_{YY} = \left[-\frac{(n-1)}{2n} D_p^{\frac{1}{n}} \right]_{YY}, \quad (78)$$

hence the inner behavior of $\hat{\Psi}_I \sim -\frac{n-1}{4n} D_p^{\frac{1}{n}} Y^2$. The analysis for $\hat{\Psi}_D$ follows in a similar manner. Thus we obtain the inner solution

$$\begin{aligned} \psi_{\text{inner}} = & \sin(\theta_\infty) X + \mathcal{E}^{-2} (A^+ X^3 + \cos(\theta_\infty) Y) + \mathcal{E}^{-4} B^+ X^3 Y \\ & + \mathcal{E}^{-4-\frac{2}{n}} \frac{1}{2} D_p^{\frac{1}{n}} Y^2 - \mathcal{E}^{-6+\frac{2}{n}} \frac{n-1}{4n} D_p^{\frac{1}{n}} Y^2 \\ & + \mathcal{E}^{-6-\frac{2}{n}} \frac{(n+1)(2n+1)}{6n^2} X^{1-\frac{1}{n}} D^+ Y^3. \end{aligned} \quad (79)$$

The above expression is uniformly valid, and the same matching conditions as before for A^+ , A^- , ..., D^- still apply. So what has happened to the layer of order \mathcal{E}^{-n} ? In fact, it has been shifted to where $C_p Y + D_p = 0$. The breakdown can be seen to occur here as $\Psi_{YY} \sim \bar{Y}^{-\frac{1}{n}}$, and $\Psi_I \sim \bar{Y}^{-\frac{1}{n}}$ where $\bar{Y} = Y + D_p/C_p$. This breakdown can be fixed in the same way as before.

6. Decaying effects

6.1. Newtonian case

In the far-field approximation, we found that the Carreau effects decayed like r^{-1} , (as $r \rightarrow \infty$) but a key question is whether or not this will be the dominant correction? The problem can be seen by noting that expression (15) is not the only solution to the biharmonic equation that satisfies the boundary conditions. In fact, there are infinitely many solutions that can be written in the form $\psi \sim \psi_0 + \sum_\lambda r^\lambda f(\theta)$, where λ is an eigen-value which, for a corner of angle α , satisfies

$$\sin((\lambda-1)\alpha) \pm (\lambda-1)\sin(\alpha) = 0, \quad (80)$$

where \pm is positive for an even mode and negative for an odd mode [2]. As we require finite behavior in the far field we have the condition $\Re(\lambda) < 0$. These extra degrees of freedom come from the fact that the behavior near to the corner is not specified.

The eigen-modes decay slower than the leading order Carreau effects if $\Re(\lambda) < -1$. We can find the eigen-values by numerically solving (80). The leading order negative eigen-value is shown in Figs. 8 and 9. Thus, the far field Carreau analysis is applicable for $\alpha < 2.2$ rad and further deviation shown in Fig. 2(a) cannot be explained by the excitation of a slowly decaying eigen-mode.

6.2. Non-Newtonian case

For the near-corner power-law system, it is also important to investigate whether Carreau fluid effects would be masked by the decay of far field disturbances. We thus search for a stream-function in the form

$$\psi = r g_0(\theta) + r_1^\lambda g_{\lambda_1}(\theta) + r^{1/2} g_{\lambda_2}(\theta) + \dots, \quad (81)$$

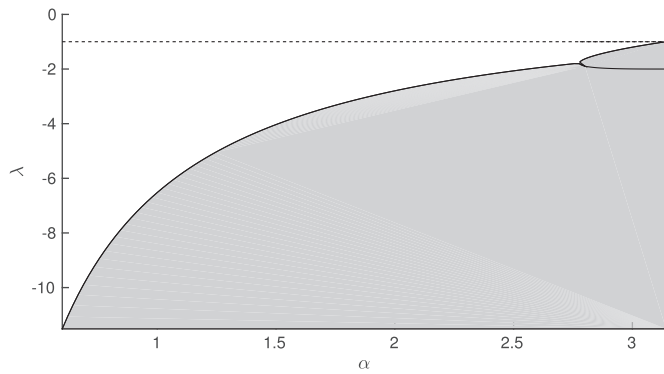


Fig. 8. Newtonian eigen-values plotted against α for an odd eigen-function (symmetric flow) excitation. The shaded region indicates where the Carreau correction is applicable.

where $1 < \lambda_1 < \lambda_2 < \dots$ and g_0 is the solution to Eq. (32). The additional terms are the modes that are excited from behavior far from the corner region. As we are only interested in the slowest decaying mode λ_1 , for ease of notation we let $\lambda = \lambda_1$, and as shear thinning fluids are much more prevalently found in nature, we present the eigen-value problem only for $n < 1$. Substituting (81) into (7) and (8) and taking leading order in r as $r \rightarrow 0$ gives rise to the eigen-value problem

$$\left\{ -\frac{\partial^2}{\partial \theta^2} + (\lambda + 1 - n)(\lambda - 1 - n) \right\} \left(n |\sin(\sqrt{n(2-n)}(\theta - \theta_\infty))|^{1-\frac{1}{n}} (g'_\lambda - \lambda(\lambda - 2)g_\lambda) \right) - 4(\lambda - n)(\lambda - 1) \left[|\sin(\sqrt{n(2-n)}(\theta - \theta_\infty))|^{1-\frac{1}{n}} g'_\lambda \right] = 0. \quad (82)$$

Classically such eigen-value problems are solved numerically by using a shooting method. However, one can see that locally, around $\theta = \theta_\infty$, the non-differentiable functions cause difficulties with ODE solvers. We thus decided to solve the problem using a Frobenius series approach. To simplify the problem we assumed that $\sin(\sqrt{n(2-n)}(\theta - \theta_\infty))$ is well approximated by $\sqrt{n(2-n)}(\theta - \theta_\infty)$. Under this assumption the general solutions can be found analytically with the eigen-value problem being expressed as a root-solving problem. The root-solving is performed using a Newton–Raphson method and the initial value is found by iterating from the Newtonian solution. The effect of n on the Newtonian even and odd modes is shown in Fig. 10, although it should be noted that for $n \neq 1$ the eigen-functions are no-longer strictly even or odd. This is to be expected as, due to non-linearity, the eigen-functions couple to the leading order behavior, which does not have such a symmetry. One can see from Fig. 10 that for $n < 0.76$, $\Re(\lambda) < 3$.

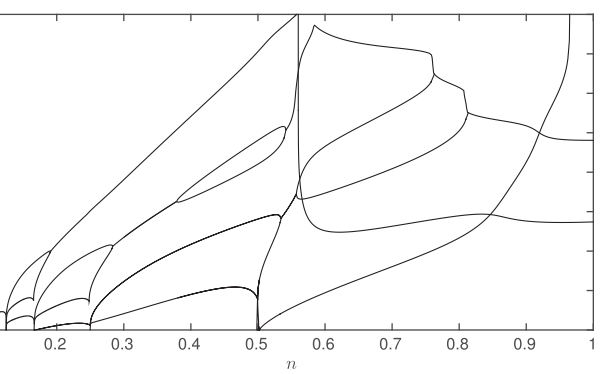
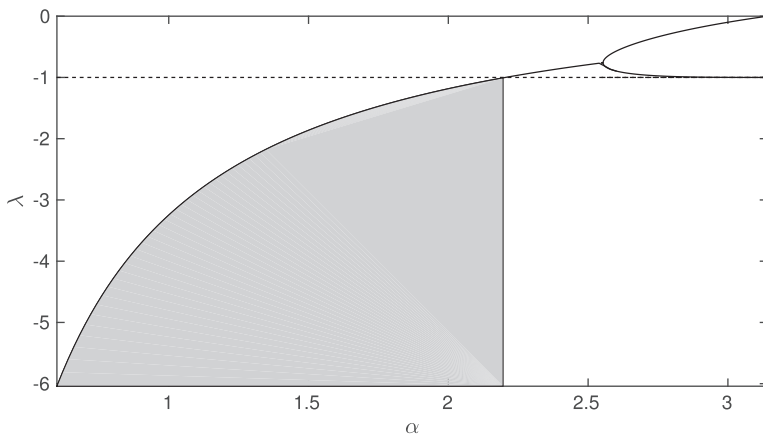


Fig. 10. The real part of the eigen-value for the non-Newtonian problem (Eq. (82)) at an angle of $\alpha = \frac{\pi}{2}$.

7. Conclusions and discussion

We find that for a Carreau fluid in a wall driven corner the radial scale determines the dominant physics of the problem, therefore we introduce the scaling that r is $\mathcal{O}(\mathcal{E}^{-1})$. Far from the corner ($\mathcal{E} \rightarrow 0$) the solution can be readily calculated and that the result correctly predicts the overshoot and undershoot of streamlines for shear thinning/thickening behaviors, respectively, though the solution is no longer valid for small r . However, the far from wall approximation will eventually breakdown due to the inertia terms becoming appreciably large. In the limit of large \mathcal{E} , that is highly shear dependent behavior, we found that the system can be modeled as a pure power-law solution in part of the domain. However, this solution breaks down along the line of zero shear and a novel boundary layer equation is required to overcome this problem. The thickness of the region in which the solution breaks down is found to be of the order \mathcal{E}^{-n} , with another change in behavior at \mathcal{E}^{-2} . This suggests that the stresses of shear thinning fluids with small power-law index n near a region of low shear rates could vary greatly from those predicted by a pure power-law fluid. The need to separate into different length scales arises in the driven corner flow problem due to the fact that the moving wall boundary condition forces the stream function to behave as r , which precludes a self-similar solution as the shear rate is radially dependent. However, if one considers the flow caused by constant shear stress (Fig. 11), as performed by Moffatt [2] in the Newtonian case, there is no radial dependence on the shear rate and a global self-similar solution can be found. We seek a solution of the form $\psi \sim \tau_0 \mu_0^{-1} r^2 f(\theta)$ whereby the stress tensor components reduce to

$$\tau_{rr} = 2\mu f' = -\tau_{\theta\theta}, \quad \tau_{r\theta} = \mu f'', \quad (83)$$

with the shear rate as given by Eq. (9),

$$\dot{\gamma} = \tau_0 \mu_0^{-1} (f'^2 + 4f''^2)^{\frac{1}{2}}, \quad (84)$$

Fig. 9. Newtonian eigen-values plotted against α for an even eigen-function (anti-symmetric flow) excitation. The shaded region indicates where the Carreau correction is applicable.

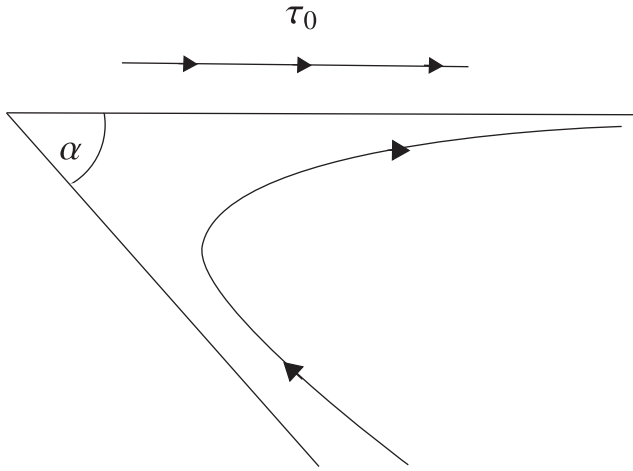


Fig. 11. Sketch of the shear driven flow problem.

whence the viscosity simplifies to

$$\mu = \mu_0(1 + (\Gamma\tau_0\mu_0^{-1})^2(f''^2 + 4f'^2))^{\frac{n-1}{2}}. \tag{85}$$

The momentum Eq. (7), after introducing a similar scaling approach as used in (4) to remove inertia, reduces to the non-linear ODE

$$\frac{d^2}{d\theta^2} \left\{ (1 + (f''^2 + 4f'^2))^{\frac{n-1}{2}} f'' \right\} + 4 \frac{d}{d\theta} \left\{ (1 + (f''^2 + 4f'^2))^{\frac{n-1}{2}} f' \right\} = 0. \tag{86}$$

When Eq. (86) is solved subject to a constant shear stress being applied at some angle α and a no-slip condition on the bottom wall it gives the constraints

$$f(0) = f(\alpha) = f'(0) = 0, \quad (1 + (f''(\alpha)^2 + 4f'(\alpha)^2))^{\frac{n-1}{2}} f''(\alpha) = 1. \tag{87}$$

As no analytic solution could be found we solved (87) using the shooting method in conjunction with a Runge–Kutta 4 solver. The

Appendix A. Exact solution for power-law correction.

For the parameter choice $n = 3$ the general solution for the correction to the power-law Eq. (38) can be found in terms of tabulated functions. For $n = 3$, the governing equation simplifies to

$$\left(\frac{d^2}{d\theta^2} + 1 \right) \{ 3(g_0 + g_0'')^2 (g_1'' - 3g_1) + \kappa_p |g_0 + g_0''| \} = 0. \tag{A.1}$$

This can be solved by the same means as Eq. (35) which leads to the exact solution

$$g_1 = A \sinh(\sqrt{3}(\theta - \theta_\infty)) + B \cosh(\sqrt{3}(\theta - \theta_\infty)) + CI_1(\theta) + DI_2(\theta). \tag{A.2}$$

The functions I_1 and I_2 are given by:

$$I_1(\theta) = e^{-\sqrt{3}\theta} \int e^{\sqrt{3}\theta} \sinh^{-\frac{2}{3}}(\sqrt{3}(\theta - \theta_\infty)) \sin(\theta - \theta_\infty) d\theta - e^{\sqrt{3}\theta} \int e^{-\sqrt{3}\theta} \sinh^{-\frac{2}{3}}(\sqrt{3}(\theta - \theta_\infty)) \sin(\theta - \theta_\infty) d\theta, \tag{A.3}$$

$$I_2(\theta) = e^{-\sqrt{3}\theta} \int e^{\sqrt{3}\theta} \sinh^{-\frac{2}{3}}(\sqrt{3}(\theta - \theta_\infty)) \cos(\theta - \theta_\infty) d\theta - e^{\sqrt{3}\theta} \int e^{-\sqrt{3}\theta} \sinh^{-\frac{2}{3}}(\sqrt{3}(\theta - \theta_\infty)) \cos(\theta - \theta_\infty) d\theta. \tag{A.4}$$

Appendix B. Inner behavior of the outer solution

The solution to Eq. (38) was obtained by use of Frobenius series, and is required to give the additional terms needed to describe the behavior far from $\theta = 0$. However, the leading order terms could be computed in a more direct manner, and as the equation appears later in the matching process we include it. If one considers the case where θ is small, then the second order derivatives dominate Eq. (38). Keeping the highest order derivatives for the homogeneous and inhomogeneous parts one finds that

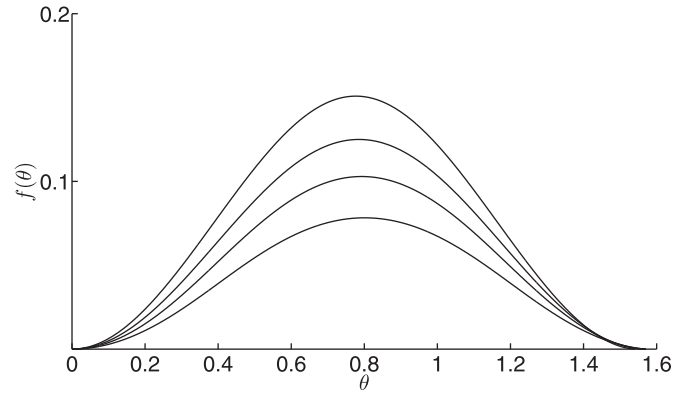


Fig. 12. The function f for the shear-driven case. The results are shown, from bottom to top, for $n = 0.2, 0.5, 1, 2$.

results are presented in Fig. 12. One might have considered applying a similar matching approach to that used for the driven corner problem to this system. However, one can see from Eq. (84) that zero shear can only occur when there is no curvature and gradient in f . From the graph in Fig. 12, we can see that this scenario never occurs, thus no break-down will occur.

The regions of applicability for both the near-field and far-field analysis were found. The far-field Carreau correction is found to be of greater importance than the eigen-modes for angles less than ≈ 2.2 rad. However, for larger angles, the decay from the near corner effects are more prevalent. A similar study was performed for the near-region. We concluded that, other than for weakly shear-thinning fluids, the far field eigen-modes are more important except for in the boundary layer region.

Acknowledgment

This work was supported by funding from the EPSRC grant EP/I019790/1.

$$\frac{d^2}{d\theta^2} \{n|g_0 + g_0''|^{n-1}g_1'' + \kappa_p |g_0 + g_0''|^{n-2}\} = 0. \quad (\text{B.1})$$

Using only the first order term for $g_0'' + g_0 = C_0\theta^{\frac{1}{n}}$, Eq. (B.1) reduces to,

$$\left[|\theta|^{1-\frac{1}{n}}g_1''\right]'' = -\frac{1}{n}\kappa_p C_0^{-1} \left(|\theta|^{1-\frac{2}{n}}\right)'', \quad (\text{B.2})$$

which appears ubiquitously throughout the matching process. We can integrate (B.2) to give

$$g_1 = A + B\theta + C\theta^{1+\frac{1}{n}} + D\theta^{2+\frac{1}{n}} - \frac{n}{2(2n-1)} \left|K_1(\alpha) \left(n^{\frac{1}{2n}}(n-2)^{\frac{1}{2n}}\right)^{-1} \text{sgn}(\theta) |\theta|^{2-\frac{1}{n}}\right|. \quad (\text{B.3})$$

References

- [1] W.R. Dean, P.E. Montagnon, On the steady motion of viscous liquid in a corner, *Mathematical Proceedings of the Cambridge Philosophical Society* 45 (1949) 389–394, <http://dx.doi.org/10.1017/S0305004100025019>.
- [2] H.K. Moffatt, Viscous and resistive eddies near a sharp corner, *Journal of Fluid Mechanics* 18 (1964) 1–18, <http://dx.doi.org/10.1017/S0022112064000015>.
- [3] S. Taneda, Visualization of separating stokes flows, *Journal of the Physical Society of Japan* 46 (6) (1979) 1935–1942, <http://dx.doi.org/10.1143/JPSJ.46.1935>.
- [4] I. Proudman, M. Asadullah, Steady viscous flow near a stationary contact line, *Journal of Fluid Mechanics* 187 (1988) 35–43, <http://dx.doi.org/10.1017/S0022112088000321>.
- [5] P. Henriksen, O. Hassager, Corner flow of power law fluids, *Journal of Rheology* 33 (6) (1989) 865–879 <https://doi.org/10.1122/1.550039>.
- [6] R. Keiller, E. Hinch, Corner flow of a suspension of rigid rods, *The Journal of Non-Newtonian Fluid Mechanics* 40 (3) (1991) 323–335 [https://doi.org/10.1016/0377-0257\(91\)87016-Q](https://doi.org/10.1016/0377-0257(91)87016-Q).
- [7] G. Taylor, On scraping viscous fluid from a plane surface, *The Scientific Papers of Sir Geoffrey Ingram Taylor*, 4 Cambridge University Press, London, 1962, pp. 410–413.
- [8] C. Hancock, E. Lewis, H.K. Moffatt, Effects of inertia in forced corner flows, *Journal of Fluid Mechanics* 112 (1981) 315–327, <http://dx.doi.org/10.1017/S0022112081000426>.
- [9] C. Hills, H.K. Moffatt, Rotary honing: a variant of the Taylor paint-scraper problem, *Journal of Fluid Mechanics* 418 (2000) 119–135, <http://dx.doi.org/10.1017/S0022112000001075>.
- [10] G. Tatterson, R. Brodkey, R. Calabrese, Move mixing technology into the 21st century, *Chemical Engineering Progress* 87 (6) (1991) 45–48.
- [11] R. Layton, W. Murray, J. Garbini, The control of power for efficient batch mixing, *Propellants Explosives Pyrotechnics* 22 (5) (1997) 269–278, <http://dx.doi.org/10.1002/prop.19970220505>.
- [12] J. Riedler, W. Schneider, Viscous flow in corner regions with a moving wall and leakage of fluid, *Acta Mechanica* 48 (1–2) (1983) 95–102, <http://dx.doi.org/10.1007/BF01178500>.
- [13] Y. Huang, R. Bhatnagar, K. Rajagopal, Flow of a non-newtonian fluid between intersecting planes of which one is moving, *Rheologica Acta* 32 (5) (1993) 490–498, <http://dx.doi.org/10.1007/BF00396180>.
- [14] K. Yasuda, R.C. Armstrong, R.E. Cohen, Shear flow properties of concentrated solutions of linear and star branched polystyrenes, *Rheologica Acta* 20 (2) (1981) 163–178, <http://dx.doi.org/10.1007/BF01513059>.
- [15] N.E. Marcovich, M.M. Reboledo, J. Kenny, M.I. Aranguren, Rheology of particle suspensions in viscoelastic media. Wood flour-polypropylene melt, *Rheologica Acta* 43 (3) (2004) 293–303, <http://dx.doi.org/10.1007/s00397-003-0349-0>.
- [16] G. Batchelor, *An Introduction to Fluid Mechanics*, Cambridge University Press, London, 1967.
- [17] C. Bender, S. Orszag, *Advanced mathematical methods for scientists and engineers I: Asymptotic methods and perturbation theory*, *Advanced Mathematical Methods for Scientists and Engineers*, Springer, 1978.
- [18] S. Chaffin, *Non-Newtonian fluids in complex geometries*, Ph.D. thesis University of Sheffield, 2016.
- [19] M. Renardy, A matched solution for corner flow of the upper convected Maxwell fluid, *The Journal of Non-Newtonian Fluid Mechanics* 58 (1) (1995) 83–89.
- [20] E.J. Hinch, *Perturbation Methods*, Cambridge University Press, 1991. Cambridge Books Online.